Applied Geochemistry 59 (2015) 95–103

Contents lists available at ScienceDirect

Applied Geochemistry

journal homepage: www.elsevier.com/locate/apgeochem

# Effect of exopolymers on oxidative dissolution of natural rhodochrosite by *Pseudomonas putida* strain MnB1: An electrochemical study

Huawei Wang [a,c], Daoyong Zhang [a,b], Wenjuan Song [a], Xiangliang Pan [a,*], Fahad A. Al-Misned [d], M. Golam Mortuza [d,e]

[a] Laboratory of Environmental Pollution and Bioremediation, State Key Laboratory of Desert and Oasis Ecology, Xinjiang Institute of Ecology and Geography, Chinese Academy of Sciences, Urumqi 830011, China
[b] State Key Laboratory of Environmental Geochemistry, Institute of Geochemistry, Chinese Academy of Sciences, Guiyang 550002, China
[c] University of Chinese Academy of Sciences, Beijing 100049, China
[d] Department of Zoology, College of Science, King Saud University, Riyadh 11451, Saudi Arabia
[e] Department of Zoology, Faculty of Life and Earth Science, Rajshahi University, Rajshahi 6205, Bangladesh

ARTICLE INFO

*Article history:*
Available online 5 May 2015
Editorial handling by B. Ngwenya

ABSTRACT

Oxidative dissolution of natural rhodochrosite by the Mn(II) oxidizing bacterium *Pseudomonas putida* strain MnB1 was investigated based on batch and electrochemical experiments using natural rhodochrosite as the working electrode. Tafel curves and batch experiments revealed that bacterial exopolymers (EPS) significantly increased dissolution of natural rhodochrosite. The corrosion current significantly increased with reaction time for EPS treatment. However, the corrosion process was blocked in the presence of cells plus extra EPS due to formation of the passivation layer. Moreover, the scanning electron microscopy and the energy dispersive spectroscopy (SEM–EDS) results showed that the surface of the natural rhodochrosite was notably changed in the presence of EPS alone or/and bacterial cells. This study is helpful for understanding the role of EPS in bacterially oxidation of Mn(II). It also indicates that the Mn(II) oxidizing bacteria may exert their effects on Mn(II) cycle and other biological and biogeochemical processes much beyond their local ambient environment because of the catalytically dissolution of solid Mn(II) by EPS and the possible long distance transport of the detached EPS.



## 1. Introduction

Natural rhodochrosite ($MnCO_3$) is a common Mn mineral in rock, soil and sediment. Extensive deposition of natural rhodochrosite has been found in the Northern Limestone Alps, the Molango District, the Black Sea and the central south and southwest China (Fan and Yang, 1999; Germann, 1973; Okita, 1992; Roy, 1997). Rhodochrosite is a raw material for industrial use in the production of Mn alloys, electrolytic Mn, magnetic materials and catalysts (Kosterov et al., 2006).

Oxidative dissolution of rhodochrosite to generate $Mn^{2+}$ ions and subsequently to form Mn oxides is an important pathway for the elemental Mn cycle. Under abiotic conditions, dissolution of synthetic rhodochrosite to free $Mn^{2+}$ in pure water and saline solution in aerobic or anaerobic environments has been well elaborated (Duckworth and Martin, 2004; Jensen et al., 2002; Luo and Millero, 2003; Savenko, 2005). Abiotic exhalative activities contributes to the formation of Mn(IV) oxides (Post, 1999), however, abiotic oxidation of $Mn^{2+}$ ions to Mn(IV) by $O_2$ is kinetically limited (Diem and Stumm, 1984). It is interesting that, because Mn(II) oxidizing microbes can significantly accelerate oxidation of $Mn^{2+}$, many natural Mn oxides nodules are derived from activities of these microbes (Greenslate, 1974; Miller et al., 2012; Tebo et al., 2005). These biogenic Mn oxides are involved in a range of biogeochemical reactions and play a key role in oxidation of organic matter and detainment of heavy metals (Chang et al., 2014, 2013; Jensen et al., 2002; Kim et al., 2012).

A recent study shows that biotic oxidative dissolution of natural rhodochrosite, used as the only Mn(II) source, has been substantially enhanced in the presence of Mn(II) oxidizing fungi, and the extracellular superoxide and extracellular organic molecules play a key role in the formation of Mn oxides (Tang et al., 2013). However, studies on the role of exopolymers (also extracellular polymeric substances, EPS) in oxidative dissolution of minerals have been mainly focused on natural $FeS_x$ ($1 \leqslant x \leqslant 2$) minerals (Fowler et al., 1999; Gu et al., 2013; Rohwerder et al., 2003). EPS are responsible for mediating *Acidithiobacillus ferrooxidans* attachment on minerals surface (Harneit et al., 2006; Salerno et al., 2007). A similar report shows that the primary attachment of

* Corresponding author. Tel./fax: +86 991 7823115.
*E-mail address:* panxl@ms.xjb.ac.cn (X. Pan).

http://dx.doi.org/10.1016/j.apgeochem.2015.04.015
0883-2927/

*Thiobacillus ferrooxidans* to pyrite is mediated by positively charged EPS complexed Fe(III) (Gehrke et al., 1998). In addition to the role of EPS in attachment of bacterial cells to the solid surfaces, dissolution of minerals and oxidation of Fe(II) and/or other low valence elements occurs at EPS–mineral interface was reported (Bosecker, 1997; Tributsch, 2001). In comparison with the well documented crucial role of EPS in dissolution of pyrite, the role of EPS in dissolution of rhodochrosite have been poorly understood.

The electrochemical methods, such as Tafel polarization curves and electrochemical impedance spectroscopy (EIS), have been frequently used to characterize the water–mineral interfacial processes (Alves et al., 2005; Bevilaqua et al., 2004). Tafel polarization curve provides information about mineral corrosion process and EIS can obtain adsorption kinetics and reaction mechanism on the micrometer scale (Alves et al., 2005; Bevilaqua et al., 2004; Lin and Say, 1999; Shi et al., 2005). Both techniques are ideal for monitoring anodic and cathodic electron transfer processes, including dissolution of natural minerals.

In this study, oxidative dissolution of natural rhodochrosite to generate Mn oxide in the presence of *P. putida* MnB1 and the effect of EPS were investigated using electrochemical tests and batch experiments. The solid rhodochrosite–graphite electrodes were used to obtain the Tafel curves and EIS data. The relevant electrochemical parameters were derived by fitting the Tafel and EIS data for evaluation of the effect of EPS of *P. putida* MnB1 on oxidative dissolution of natural rhodochrosite.

## 2. Materials and methods

### 2.1. Bacterium

The Mn(II) oxidizing bacterium, *Pseudomonas putida* strain MnB1 (ATCC 23,483), was supplied by the American Type Culture Collection. The bacterial cells were grown in the nutrient broth medium (peptone, 10 g $L^{-1}$; beef extract, 3 g $L^{-1}$; NaCl, 5 g $L^{-1}$; pH 6.8) at 25 °C and 120 rpm for two days and then harvested by centrifugation at 6000*g* and 4 °C for 5 min. Then the bacterial cells were washed three times with ultrapure water and re-suspended in ultrapure water for further use. For electrochemical experiments, the #279 medium (ATCC™) with pH 6.8 was used for cell incubation. The #279 medium was composed of 0.15 g $L^{-1}$ ammonium iron sulfate, 0.15 g $L^{-1}$ sodium citrate, 0.15 g $L^{-1}$, 0.075 g $L^{-1}$ yeast extract and 0.05 g $L^{-1}$ sodium pyrophosphate.

### 2.2. Preparation and characterization of EPS

EPS was extracted by high-speed centrifugation (Pan et al., 2010a, 2010b). Our previous study showed that EPS extracted with high-speed centrifugation were suitable for scientific study (Pan et al., 2010b). For EPS extraction, cells were grown in the medium at 120 rpm and 25 °C. The optical density ($OD_{600}$) of the culture was monitored daily. When the $OD_{600}$ reached 0.8, the cells were collected by centrifugation at 4300*g* × for 10 min at 4 °C to remove superfluous medium. The pellets were re-suspended in ultra-purified water and centrifuged at 20,000*g* × for 25 min at 4 °C. The suspension was filtered through a 0.22 μm acetate cellulose membrane and the filtrate was purified by 3500 Dalton dialysis membrane for 5 times every 12 h at 4 °C in the dark.

The total organic carbon (TOC) content of EPS solution was determined with a TOC analyzer (TOC-4100, Shimadzu, Japan). The content of polysaccharides was measured by the phenolsulfuric acid method (Dubois et al., 1956) and the content of proteins was measured by the Bradford-method (Bradford, 1976). The EPS solution pH was determined with a pH meter.

For collection of Fourier-transform infrared (FT-IR) spectra, the EPS solution was freeze dried and mixed with solid KBr in the ratio of 1:100. The pellets of the mixture were prepared at 8 × 1013 kg $cm^{-2}$ pressure (Zhang et al., 2006). The functional groups of EPS were analyzed with a Fourier-transform infrared (FT-IR) spectrometer (Bruker Tensor 27, Germany).

The three-dimensional excitation-emission matrix (EEM) fluorescence spectra of the EPS solution were recorded with a F-7000 Fluorescence Spectrophotometer (HITACHI, Japan). A 450-W Xenon lamp was used as the excitation source. EEM spectra were collected at 1200 nm $min^{-1}$ with an emission range of 200–550 nm by 2 nm and an excitation range of 200–400 nm by 5 nm. Both the excitation and emission slits were set to 5 nm of band-pass. The fluorescence spectrum of Milli-Q water was subtracted from the fluorescence spectra of EPS solution. The EEM data were processed by using the software SigmaPlot 10.0 (Systat, US) (Pan et al., 2010c).

### 2.3. Natural rhodochrosite

Natural rhodochrosite mineral used in this study was obtained from a Mn mine in Hunan province of China and XRD results are shown in Fig. 1. The mineral samples were ground to less than 0.15 μm for fabrication of the rhodochrosite-carbon working electrodes. XRD results showed that natural rhodochrosite was mainly composed by rhodochrosite and quartz (Fig. S1). SEM–EDS results indicated that natural rhodochrosite contains some other elements, such as Si (2.42%), Mg (2.26%) and Ca (6.58%) (Table S1). The presence of Mg and Al suggests that there were clay minerals in the rhodochrosite. In this study, the effect of these elements on batch and electrochemical experiments was not considered, and this needs further study.

### 2.4. Preparation of rhodochrosite–graphite electrode

The rhodochrosite–graphite paste working electrodes were assembled by the method reported in the previous report (Shi et al., 2005). Briefly, 0.5 g of powdered rhodochrosite was mixed with 0.5 g of graphite of spectral purity and 0.5 ml of liquid paraffin. The working electrodes were compacted on a plate glass with a working surface area of about 0.5 $cm^2$. The surface of the working electrodes was polished and then rinsed subsequently with ethanol and ultrapure water before experimental use.

### 2.5. Electrochemical experiments

A 50 ml electrochemical tank with a three electrode system was used for electrochemical tests. The reference electrode was Ag/AgCl electrode and the counter electrode was Pt electrode. The rhodochrosite-carbon electrodes were used as the working electrodes. Four different treatments based on addition or no addition of the sterile cells or/and EPS were set for electrochemical tests. (1) fresh sterile medium as control (CK), (2) fresh sterile medium with addition of *P. putida* MnB1 cells, (3) fresh sterile medium with addition of bacterial EPS, and (4) fresh sterile medium with addition of *P. putida* MnB1 cells plus extra EPS. The cells were added into the medium at a cell density of approximately $10^7$ - cells $ml^{-1}$ and EPS was added at a concentration of 65 mg $L^{-1}$ (weight units). All the electrochemical measurements began after 30 min of pre-equilibrium between the electrodes and the solutions. A Gamry Reference 600 electrochemical workstation (Gamry, USA) was used to obtain the Tafel curves and the EIS data. Tafel measurements were carried out with a potential range from −0.2 to 0.2 V at a scan rate of 5 mV $s^{-1}$. For EIS measurements, frequency ranged from 0.2 to 100,000 Hz in the presence of 10 mV AC (alternating current) voltage. All the electrochemical tests were repeated four times.

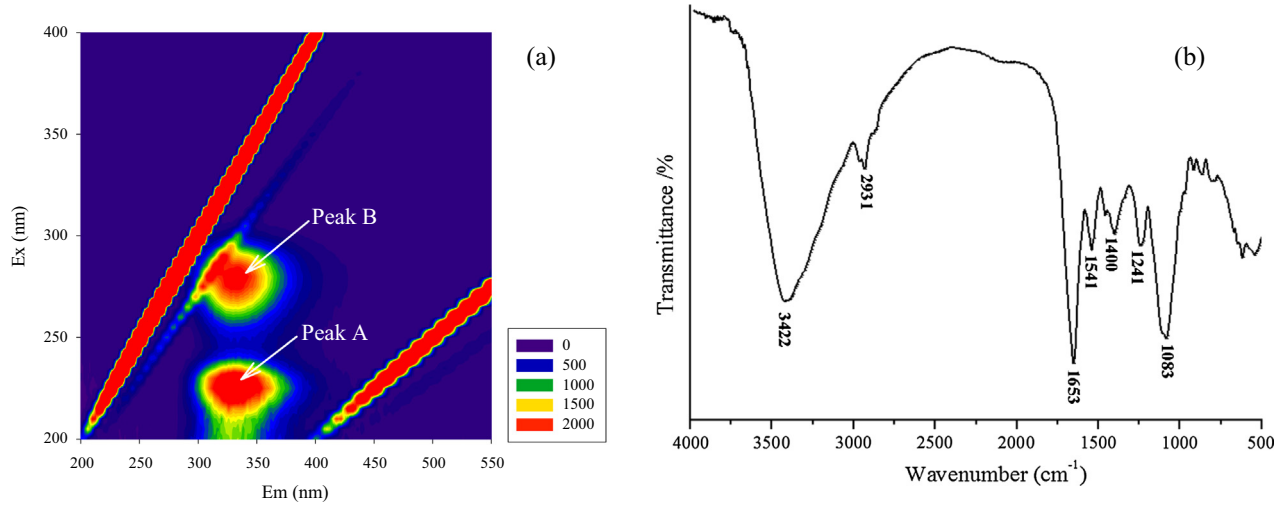


**Fig. 1.** (a) The EEM fluorescence spectrum and (b) the FTIR spectrum of EPS from *P. putida* MnB1.

### 2.6. Batch experiments

Oxidative dissolution of natural rhodochrosite was conducted in 100 ml glass bottles. Natural rhodochrosite at a dosage of 500 mg $L^{-1}$ was added into 50 ml of fresh sterile medium. Four treatments similar to the electrochemical experiments were set. For cell or/and EPS treatments, the cell density was approximately $1.6 \times 106$ cells $ml^{-1}$ and the EPS concentration was 4 mg $L^{-1}$ (TOC). The glass bottles for oxidative dissolution experiments were shaken at 200 rpm at 25 °C. Eight days after onset of the batch experiments, concentrations of $Mn^{2+}$ ions and content of Mn oxides were measured. The natural rhodochrosite samples for different treatments were also observed by SEM–EDS.

### 2.7. Analytical methods

Dissolved $Mn^{2+}$ concentration was determined by the manganese formaldehyde oxime spectrophotometry (Brewer and Spencer, 1971). Content of Mn oxide was measured by the Leukoberbelin blue (LBB) method (Okazaki et al., 1997). For SEM–EDS and XRD analysis, the samples were pretreated according to the previous study (Wang et al., 2013).

## 3. Results and discussion

### 3.1. Characterization of EPS

The extracted EPS solution pH was 6.8, with TOC, contents of proteins and polysaccharides were $51 \pm 1.52$ mg $L^{-1}$, $47.03 \pm 0.22$ μg $mL^{-1}$ and $11.12 \pm 0.04$ μg $mL^{-1}$, respectively. The EEM fluorescence spectrum showed there were two fluorescence peaks (Fig. 1a). The fluorescence of peak A (Ex about 225 nm, Em about 340 nm) and B (Ex about 275–280 nm, Em about 335 nm) were emitted from the protein-like substances containing tryptophan (Zhang et al., 2010).

The FTIR spectrum of EPS was shown in Fig. 1b. The intensive band at 3422 $cm^{-1}$ could be attributed to the stretching vibration of —OH of polysaccharides and proteins. The band at 1653 $cm^{-1}$ corresponded to the stretching vibration of amide I C=O and C—N functional groups of proteins. The 1541 $cm^{-1}$ implied the presence of the stretching vibration of C—N and deformation vibration of N—H of amide II (Pan et al., 2005). The 1400 $cm^{-1}$ band indicated the presence of the deprotonated carboxyl group (Tourney et al., 2008). The 1241 $cm^{-1}$ band could be assigned to the carboxyl group (deformation vibration of C=O and stretching vibration of OH), which combined with $CH_2$ at 2931 $cm^{-1}$ indicated the presence of uronic acid and humic acid. The presence of $CH_2$ and carboxylic groups indicated the presence of lipid, whose content is usually too low to be detected with IR spectra. The band at 1083 $cm^{-1}$ could be identified as the phosphodiester groups (Heinrich et al., 2007; Tourney et al., 2008). The bands at "fingerprint zone" less than 1000 $cm^{-1}$ indicated the presence of the phosphate group from nucleic acids (Pan et al., 2005; Zhang et al., 2006). The EEM fluorescence and FTIR spectra showed that the components of EPS were complex with proteins and polysaccharides being the dominant components.

### 3.2. Oxidative dissolution of natural rhodochrosite

Table 1 listed the dissolved $Mn^{2+}$ concentration and $MnO_2$ content of rhodochrosite untreated and treated with cells and/or EPS. For CK, the sterile medium caused release of some $Mn^{2+}$ ions from rhodochrosite but no increase of $MnO_2$ content was observed. Addition of EPS to the sterile medium increased $Mn^{2+}$ concentration by 1 mg $L^{-1}$ but $MnO_2$ content did not increase in comparison with CK, indicating that EPS can increase dissolution of rhodochrosite but cannot oxidize $Mn^{2+}$. When the bacterial cells were added, $MnO_2$ content significantly increased whether extra EPS was added or not. This means that oxidative dissolution of natural rhodochrosite by living *P. putida* MnB1 cells led to generation of Mn oxides and consumption of dissolved $Mn^{2+}$ ions. The SEM–EDS results showed that the surface structure of natural rhodochrosite was not significantly modified for CK while a large number of small particles were formed on the surface for the bacterial EPS treatment (Fig. 2 and Table S1). The SEM images showed that cells were adhered to the surface of natural rhodochrosite and the surface structure was significantly different from CK and the EPS treatment, indicating that natural rhodochrosite was effectively dissolved and oxidized by the living cells. These results indicate that living cells can effectively dissolve natural rhodochrosite and oxidize dissolved $Mn^{2+}$ ions to Mn(IV) oxides, and the bacterial EPS plays an important role in dissolution of natural rhodochrosite, which is a key step in oxidation of rhodochrosite by Mn oxidizing bacteria to Mn dioxides.

### 3.3. Tafel analysis

The Tafel polarization curves versus elapsed time for various treatments are shown in Fig. 3. For CK and the cell treatments

**Table 1**
Dissolved $Mn^{2+}$ concentration and $MnO_2$ concentration in the systems after 8 d of four treatments (control, EPS treatment, cells treatment, and cells plus EPS treatment). Experimental condition: rhodochrosite dosage, 5 g $L^{-1}$; bacterial density, 1.6 × $10^6$ cell $mL^{-1}$; EPS concentration, 4 mg $L^{-1}$ (TOC); reaction time, 8 d. All data were presented as the average of triplicates ± standard errors.

| Mn content | Original rhodochrosite | CK | EPS alone treatment | Cells treatment | Cells plus extra EPS treatment |
|---|---|---|---|---|---|
| Dissolved $Mn^{2+}$ ions (mg $L^{-1}$) | /[a] | 2.62 ± 0.08 | 3.67 ± 0.15 | 0.34 ± 0.04 | 0.16 ± 0.02 |
| $MnO_2$ (mg $L^{-1}$) | 1.10 ± 0.04 | 1.13 ± 0.15 | 1.12 ± 0.08 | 20.77 ± 2.06 | 19.22 ± 1.04 |

*Note:* "a" represents the content of dissolved $Mn^{2+}$ ion before experiments was negligible.

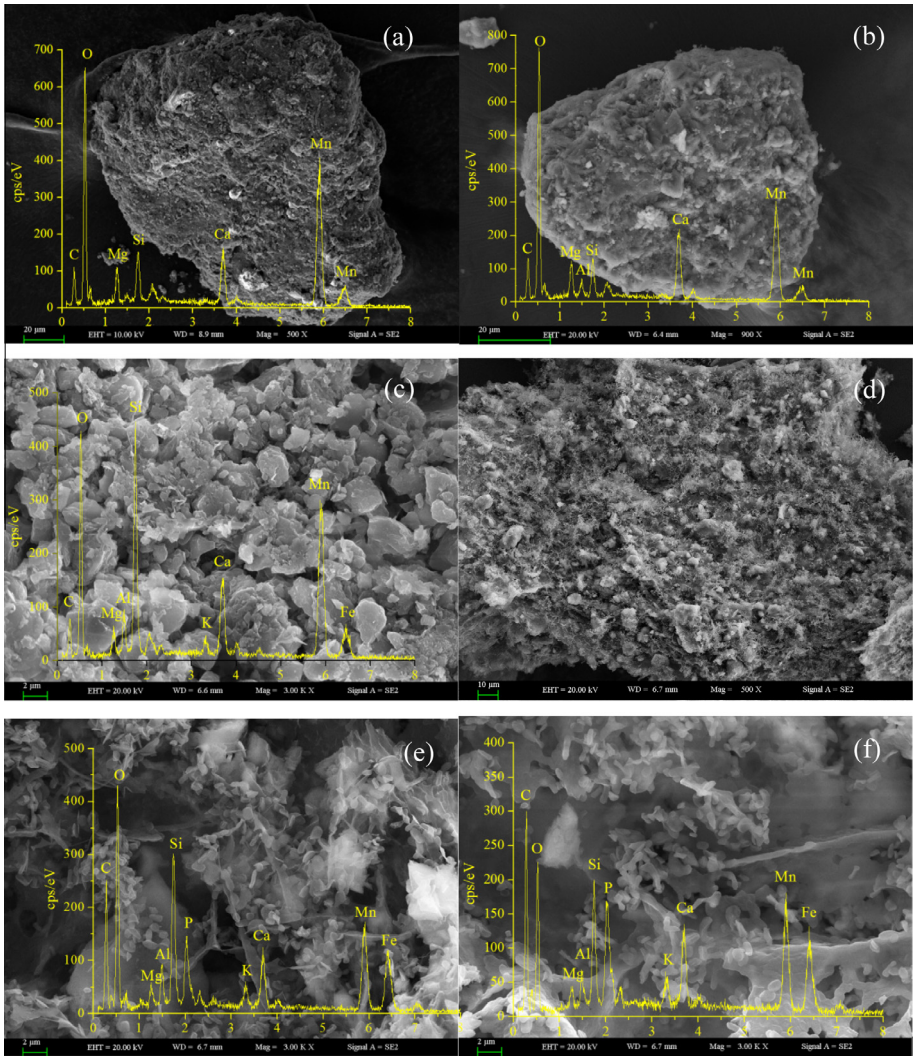


**Fig. 2.** Comparison of SEM–EDS spectra of natural rhodochrosite under different systems: (a) pristine natural rhodochrosite (×500); (b) sterile CK (×900); (c) EPS treatment (×3000); (d) cell treatment (×500); (e) cell treatment (×3000); (f) cell and extra EPS treatment (×3000).

(Fig. 3a and c), corrosion potential of the electrodes decreased with time and the curves generally shifted downward with time. However, the curves firstly moved downward and then shifted upward in the presence of high concentrations of EPS (Fig. 3b). The curves shifted mostly positive for treatment with cells plus extra EPS (Fig. 3d). The negative shift of corrosion potential suggests that reaction activation energy decreased and this will promote the dissolution or chemical reaction (Gu et al., 2012). On the contrary, the positive shift of corrosion potential implies the existence of corrosion products on electrode surface, which acts as a physical barrier and thus will inhibit the damage of corrosive medium to the electrode surface. Moreover, upward shift of the curves indicates the increasing corrosion current density and this would increase the corrosion rate of electrode surface.

The corrosion parameters ($E_{corr}$ and $I_{corr}$) were estimated from the Tafel polarization curves (Fig. 4). Corrosion potential and corrosion current for the sterile treatment gradually decreased with elapsed time. Corrosion process for the sterile treatment was mainly due to the dissolution of natural rhodochrosite to $Mn^{2+}$ ion. The decreasing corrosion rate of rhodochrosite was caused by the passivation of electrodes surface (Lopez-Juarez et al., 2006; Zeng et al., 2011). For cell treatment, corrosion potential decreased with corrosion time, but corrosion current did not decrease and was observed as relatively high values (269–362 nA) for a long time (0–8 d). This indicates that no passivation layer of electrodes on the mineral surface is formed in the presence of living cells. For EPS treatment, corrosion potential was significantly lower in comparison with the other treatments at the initial stage (0–3 d) and

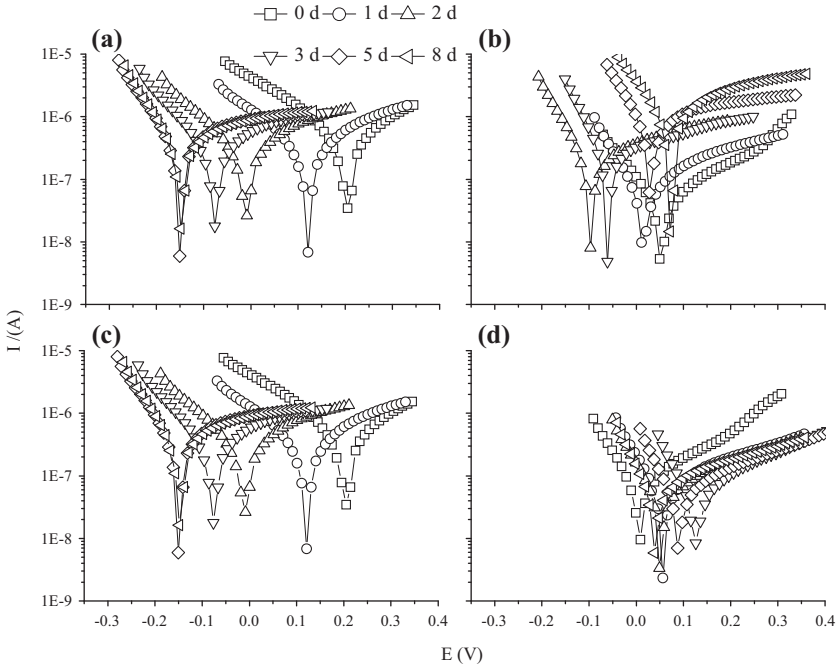


**Fig. 3.** Changes of Tafel polarization curves with corrosion time of different systems: (a) CK; (b) EPS treatment; (c) cells treatment; (d) cells and extra EPS treatment. Experimental condition: bacteria density, $1.0 \times 10^7$ cell $mL^{-1}$; EPS concentration, 65 mg $L^{-1}$; reaction time, 8 days; scan rate, 5 mV $s^{-1}$; potential, −0.2 to 0.2 mV.

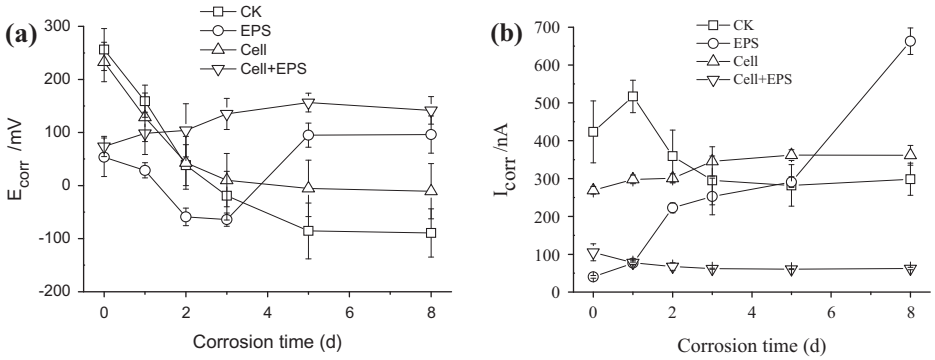


**Fig. 4.** The changes of corrosion parameters versus elapsed time with different treatment: (a) corrosion potential ($E_{corr}$) and (b) corrosion current ($I_{corr}$). The corrosion parameters were obtained by fitting the experimental results with the software of Gamry reference 600. Standard errors represent four triplicates.

thereafter increased to about 100 mV. At the third day, the value was lowest (−64 ± 12.4 mV), which could be attributed to the dissolution of rhodochrosite electrode. Meanwhile, the corrosion current was significantly increased with reaction time. At the end of the experiment (8 d), the value of corrosion current was 663 ± 35 nA, which was higher than the values for the other treatments. These results suggest that bacterial EPS plays an important role in enhancing dissolution of natural rhodochrosite. Gehrke et al. (1998) also showed that EPS from *T. ferrooxidans* was responsible for attachment to pyrite surface, increasing hydrophobic properties and complexation with Fe(III) ions. Harneit et al. (2006) also confirmed that EPS from four strains of *A. ferrooxidans* was responsible for mediating of mineral dissolution.

Corrosion of the electrode was significantly retarded when cells and extra EPS were added. The inhibitory effect on corrosion was mainly attributed to the presence of high concentration of EPS, cells and bacterial Mn oxides. EPS was involved in the dissolution of natural rhodochrosite to generate $Mn^{2+}$ ions and then the living cells oxidized $Mn^{2+}$ ions to form layered Mn oxides on the surface of natural rhodochrosite (Tang et al., 2013). For cell treatment, no significant inhibitory effect was observed. However, the insoluble products such as bacterial Mn oxides formed during the dissolution of rhodochrosite would remain on the electrode surface together with EPS to form a passivation layer of rhodochrosite. It has been reported that during microbial leaching of chalcopyrite, insoluble $S^0$ and jarosite and bacterial EPS remained on the surface of chalcopyrite and generated a tight passivation layer (Zeng et al., 2010). The layer would block the flow of microbial nutrients (such as C source and $Mn^{2+}$ ions) and reaction products across the electrode–water interface and lead to the inhibition of corrosive dissolution (Hackl et al., 1995; Watling, 2006).

### 3.4. EIS analysis

The EIS spectra of the rhodochrosite electrodes in the form of Nyquist plots are shown in Fig. 5. For CK and the cell treatment, the impedance spectra show an incomplete semicircle shape within two days and this indicates that dissolution of rhodochrosite is mainly controlled by a charge transfer process. Two d after onset of the experiments, EIS spectra were characterized with

incomplete semicircles at high frequency followed by a nearly 45° line at low frequency, which implies that the corrosion is controlled by both electron transfer process at high frequency and solid diffusion-limited process at low frequency (Gu et al., 2012; Shi et al., 2005). For CK and the cell treatment, the impedance showed an increasing trend with corrosion time and the semicircle became stable for CK after one day of reaction. For the cells plus extra EPS treatment, the impedance was much higher than the other treatments. This implies that the passive film was formed on the surface of electrode and the layer retarded dissolution of rhodochrosite.

For the EPS treatment, the EIS curve shape was similar to those for the other treatments, but the radius of the semicircles firstly increased and then decreased quickly, which indicates enhanced dissolution of rhodochrosite. The depressed semicircle at day 5 and 8 was caused by the uneven distribution of the electric field on the electrode–solution interface (Lin and Say, 1999). The small semicircles at high frequency were followed by oblique lines. The semicircle at high frequency can be attributed to the electrode-solution interfacial capacitance and the charge transfer resistance of electrochemical reaction. An oblique line at low frequency is the characteristics of Warburg impedance and represents the mass transfer resistance caused by the diffusion of oxidizing agents or products (Bonora et al., 1996; Liu et al., 2011; Zeng et al., 2011).

The equivalent circuits $R_s(Q(R_{ct}Z_W))$ and $R_s(Q(R_{ct}))$ were used to fit the EIS data (Fig. S2), where $R_s$ represents the solution resistance, $R_{ct}$ is the polarization resistance of charge transfer, $Z_w$ is the Warburg impedance component, and $Q$ is the constant phase element which is related to capacitor of the double-layer of the electrode and electrolyte interface.

The impedance spectra of rhodochrosite electrode for different treatments were well fitted with the above mentioned equivalent circuits (Fig. 6), which suggests that the proposed equivalent circuits can satisfactorily describe the electrochemical behavior of rhodochrosite. The EIS parameters of electrodes for different treatments except for the cells plus EPS treatment were listed in Table 2. For CK, the cell treatment and the EPS treatment, the very low $\chi^2$ of $10^{-4}$, representing the sum of quadratic deviations between experimental and simulated data, over entire corrosion time indicates that the proposed circuit is suitable for describing the impedance spectra. $Y_o$ and $n$ are the frequency independent parameters. $Y_o$ showed different trends with corrosion time. $Y_o$ decreased with reaction time for CK but it first increased and then decreased for the EPS treatment. $Y_o$ for the EPS treatment was comparatively lower than that for the other treatments. The value of $n$ reflects the surface heterogeneities and roughness of the electrode and the differences of $n$ for different treatments were also observed. The higher $n$ values for the EPS treatment might result from the attachment of EPS or the precipitation of reaction products (Schiller and Strunz, 2001). In addition, $R_s$ for the cell treatment was lower than CK and the EPS treatment (Table 2), indicating that more $Mn^{2+}$ ions dissolved from rhodochrosite were oxidized by living bacterial cells. $R_{ct}$ firstly increased and then decreased with corrosion time. The increase of $R_{ct}$ is attributed to the formation of the passive film on electrode surface in the initial stage of dissolution of rhodochrosite while the decrease of $R_{ct}$ is due to the damage to the passive film. $R_{ct}$ for the EPS treatment was significantly lower than that for the other two treatments. This means that EPS contributed to the dissolution of rhodochrosite. The EIS results are consistent with the Tafel analysis data.

The results of batch experiments, electrochemical tests and SEM–EDS analysis consistently showed that EPS from *P. putida* MnB1 increased dissolution of natural rhodochrosite but cannot catalyze oxidation of $Mn^{2+}$. The proposed rhodochrosite oxidation mechanisms of *P. putida* MnB1 can be the accelerating dissolution of rhodochrosite and release of $Mn^{2+}$ by EPS and subsequent oxidation of $Mn^{2+}$ to Mn oxides by the living bacterial cells. However, the oxidative dissolution of natural rhodochrosite could be inhibited due to the Mn oxides passivation layers on the surface produced by the living bacterial cells.

### 3.5. Environmental implication

Mn(II) oxidation catalyzed by microbes such as Mn(II)-oxidizing bacteria is several orders of magnitude faster than either abiotic catalysis on mineral surfaces or homogeneous oxygenation in aqueous solution (Tebo et al., 2004). Because of the abundant Mn oxides and ubiquitous Mn(II) oxidizing bacteria in terrestrial and marine environments, this microbially Mn(II) oxidation is a key process that affect many other important biological and geochemical processes

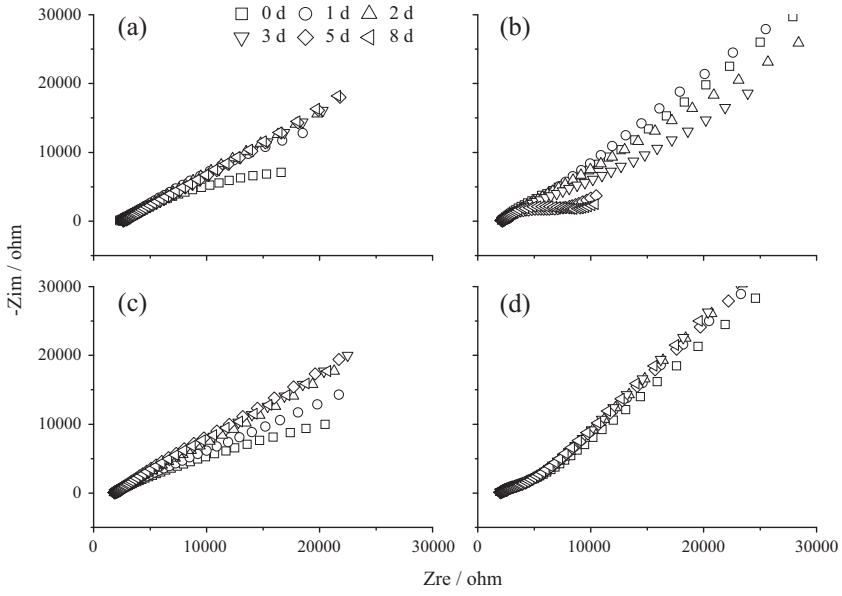


**Fig. 5.** Nyquist plots of rhodochrosite–graphite paste electrode with different treatments: (a) CK; (b) EPS treatment; (c) cells treatment; (d) cells and extra EPS treatment. Experimental condition: Bacteria density, $1.0 \times 10^7$ cell $mL^{-1}$; EPS concentration, 65 mg $L^{-1}$; reaction time, 8 days; alternating current, 10 mV; frequency, 0.2–100,000 Hz.

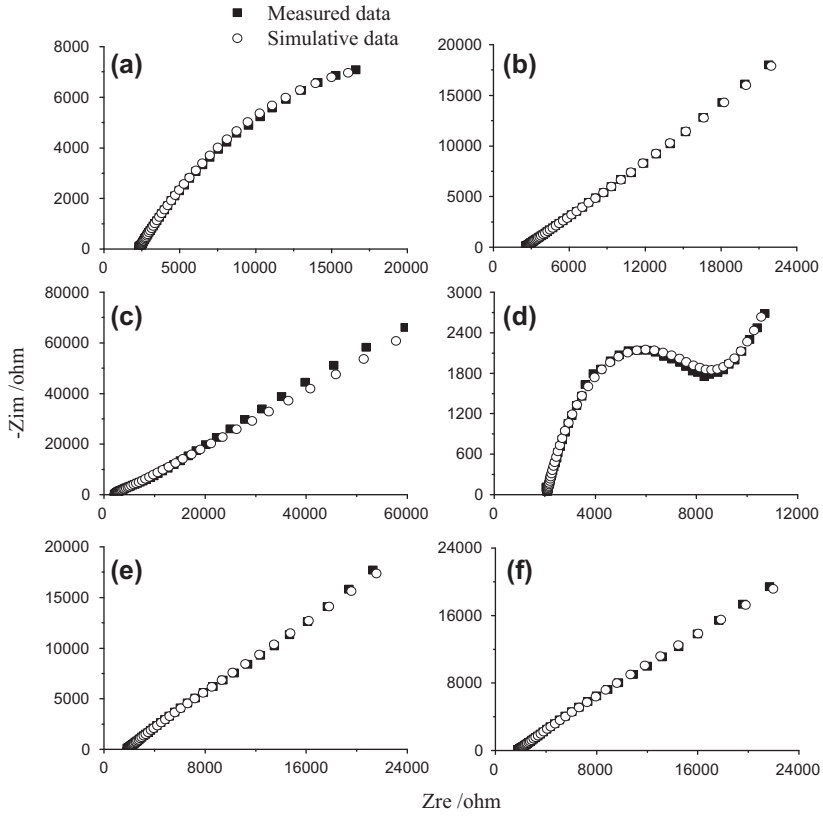


**Fig. 6.** Experimental and simulated Nyquist plots under different system: (a) CK at 0 d; (b) CK at 5 d; (c) EPS treatment at 0 d; (d) EPS treatment at 8 d; (e) Cells treatment at 2 d; (f) Cells treatment at 5 d. The simulative results were obtained by fitting the measured data with the software of ZSimwin 3.30. Standard errors represent four triplicates.

**Table 2**
Impedance parameters for electrodes with different treatments (%SD). Experimental condition: Bacteria density, $1.0 \times 10^7$ cell $mL^{-1}$; EPS concentration, 65 mg $L^{-1}$; reaction time, 8 days. Standard errors represent four triplicates.

| *T* | day | $R_s$ (Ω) | $Y_o/10^{-6}$ (S $s^n$) | *n* | $R_{ct}$ (Ω) | $W/10^{-6}$ (S $s^n$) | $\chi^2/10^{-4}$ |
|---|---|---|---|---|---|---|---|
| CK | 0[a] | 2306 (0.27) | 36.5 (1.20) | 0.50 (0.56) | 34,570 (2.42) | / | 1.17 |
| | 1[a] | 2368 (0.26) | 38.1 (1.02) | 0.51 (0.51) | 119,400 (7.05) | / | 1.19 |
| | 2 | 2396 (0.22) | 31.6 (4.64) | 0.50 (1.27) | 26,530 (25.27) | 7.8 (19.60) | 0.22 |
| | 3 | 2538 (0.19) | 30.1 (2.72) | 0.49 (0.79) | 23,300 (10.75) | 8.6 (11.05) | 0.23 |
| | 5 | 2547 (0.17) | 27.1 (2.38) | 0.49 (0.68) | 25,670 (9.47) | 8.1 (9.21) | 0.17 |
| | 8 | 2582 (0.19) | 25.9 (3.02) | 0.52 (0.87) | 35,420 (14.61) | 10.3 (8.02) | 0.23 |
| Cells | 0 | 1851 (0.62) | 26.3 (3.94) | 0.48 (1.38) | 35,530 (9.74) | 78.1 (16.9) | 3.61 |
| | 1 | 1915 (0.41) | 24.4 (3.34) | 0.51 (1.07) | 37,170 (10.38) | 29.5 (5.33) | 1.71 |
| | 2 | 1833 (0.31) | 27.4 (2.68) | 0.51 (0.86) | 70,090 (18.20) | 13.1 (7.54) | 1.02 |
| | 3 | 1839 (0.31) | 27.1 (2.12) | 0.51 (0.71) | 133,900 (25.00) | 8.9 (12.91) | 0.67 |
| | 5 | 1789 (0.33) | 27.1 (1.91) | 0.54 (0.65) | 113,800 (17.99) | 13.7 (12.66) | 1.58 |
| | 8 | 1786 (0.28) | 24.3 (2.32) | 0.54 (0.73) | 74,840 (15.51) | 13.1 (6.67) | 0.96 |
| EPS | 0 | 2130 (0.55) | 2.35 (15.72) | 0.69 (2.58) | 7055 (14.65) | 9.89 (3.55) | 2.48 |
| | 1 | 2188 (0.28) | 5.95 (12.15) | 0.62 (2.10) | 3793 (12.49) | 13.49 (4.74) | 0.15 |
| | 2 | 2234 (0.29) | 12.40 (5.43) | 0.57 (1.21) | 18,800 (13.65) | 10.40 (5.94) | 0.57 |
| | 3 | 2149 (0.33) | 10.10 (4.65) | 0.61 (1.12) | 12,430 (5.12) | 28.10 (1.62) | 1.32 |
| | 5 | 2113 (0.37) | 8.03 (4.79) | 0.65 (1.14) | 5463 (1.73) | 177.2 (2.10) | 1.88 |
| | 8 | 2083 (0.36) | 6.99 (3.93) | 0.68 (0.94) | 6783 (1.39) | 274.8 (3.65) | 2.10 |

*Note:* "a" represents the parameters obtained by the fitting of equivalent circuit $R_s(Q(R_{ct}))$.

of other elements such as C, S and Fe, especially in oxic–anoxic transition zones or at hydrothermal vents (Tebo et al., 2005). For example, Mn is a vital element of oxygen evolution complex in photosystem II, and the availability of Mn(II) to photosynthetic organisms would significantly affect the photosynthesis performance. The microbially Mn(II) oxidation may have far-reaching effects on transport and behavior of heavy metals because Mn oxides usually have strong adsorption capacity for heavy metal(loid)s. In addition, Mn oxides are strong oxidizing agents next to oxygen and can decompose a number of organic pollutants. In this study, on one hand, the catalytic dissolution of natural rhodochrosite by EPS of Mn(II) oxidizing bacteria partially elucidates the underlying mechanisms of bacterially oxidation of Mn(II). On the other hand, because most bacteria can produce copious EPS and the soluble or loosely bound EPS are easily released from the cell and transported to long distance with water (Pan et al., 2010c; Zhang et al., 2013),

this catalytic dissolution of solid Mn(II) by EPS can significantly extend the effects of Mn(II) oxidizing bacteria from local site to much farther and bigger region.

## 4. Conclusions

The effects of the Mn(II) oxidizing bacterium *P. putida* MnB1 and its EPS on oxidative dissolution of natural rhodochrosite were investigated by electrochemical tests and batch experiments. Two steps were involved in the bacterial oxidation of natural rhodochrosite. The first step is the dissolution of natural rhodochrosite and release of $Mn^{2+}$ and the bacterial EPS catalyze the dissolution of natural rhodochrosite. The second step is the bacterial oxidation of Mn(II) to Mn(IV). This study not only contributes to understanding the role of EPS in bacterially oxidation of Mn(II) but also indicates that the Mn(II) oxidizing bacteria may exert their significant effects on Mn(II) cycle and other biological and biogeochemical processes beyond their local ambient environment because of the long distance transport of the detached EPS.

## Acknowledgements

This work was supported by the West Light Foundation of Chinese Academy of Science (XBBS201304), National Natural ScienceFoundation of China (U1120302, U1403181, 21177127 and 41203088). Partial funding for this research was also received from the Visiting Professor Program at King Saud Univer-sity, Riyadh, Saudi Arabia.

## Appendix A. Supplementary material

Supplementary data associated with this article can be found, in the online version, at http://dx.doi.org/10.1016/j.apgeochem.2015.04.015.

## References

Alves, V.A., Paquim, A.M.C., Cavaleiro, A., Brett, C.M.A., 2005. The nanostructure and microstructure of steels: electrochemical Tafel behaviour and atomic force microscopy. Corros. Sci. 47, 2871–2882.
Bevilaqua, D., Diez-Perez, I., Fugivara, C.S., Sanz, F., Benedetti, A.V., Garcia, O., 2004. Oxidative dissolution of chalcopyrite by *Acidithiobacillus ferrooxidans* analyzed by electrochemical impedance spectroscopy and atomic force microscopy. Bioelectrochemistry 64, 79–84.
Bonora, P.L., Deflorian, F., Fedrizzi, L., 1996. Electrochemical impedance spectroscopy as a tool for investigating underpaint corrosion. Electrochim. Acta 41, 1073–1082.
Bosecker, K., 1997. Bioleaching: metal solubilization by microorganisms. FEMS Microbiol. Rev. 20, 591–604.
Bradford, M.M., 1976. A rapid and sensitive method for the quantitation of microgram quantities of protein utilizing the principle of protein-dye binding. Anal. Biochem. 72, 248–254.
Brewer, P.G., Spencer, D.W., 1971. Colorimetric determination of manganese in anoxic waters. Limnol. Oceanogr. 16, 107–110.
Chang, J.N., Tani, Y., Naitou, H., Miyata, N., Seyama, H., Tanaka, K., 2013. Cobalt(II) sequestration on fungal biogenic manganese oxide enhanced by manganese(II) oxidase activity. Appl. Geochem. 37, 170–178.
Chang, J.N., Tani, Y., Naitou, H., Miyata, N., Seyama, H., 2014. Sequestration of Cd(II) and Ni(II) ions on fungal manganese oxides associated with Mn(II) oxidase activity. Appl. Geochem. 47, 198–208.
Diem, D., Stumm, W., 1984. Is dissolved $Mn^{2+}$ being oxidized by $O_2$ in absence of Mn-bacteria or surface catalysts? Geochim. Cosmochim. Acta 48, 1571–1573.
Dubois, M., Gilles, K.A., Hamilton, J.K., Rebers, P.A., Smith, F., 1956. Calorimetric method for determination of sugars and related substances. Anal. Chem. 28 (3), 350–356.
Duckworth, O.W., Martin, S.T., 2004. Role of molecular oxygen in the dissolution of siderite and rhodochrosite. Geochim. Cosmochim. Acta 68, 607–621.
Fan, D.L., Yang, P.J., 1999. Introduction to and classification of manganese deposits of China. Ore Geol. Rev. 15, 1–13.
Fowler, T.A., Holmes, P.R., Crundwell, F.K., 1999. Mechanism of pyrite dissolution in the presence of *Thiobacillus ferrooxidans*. Appl. Environ. Microb. 65, 2987–2993.
Gehrke, T., Telegdi, J., Thierry, D., Sand, W., 1998. Importance of extracellular polymeric substances from *Thiobacillus ferrooxidans* for bioleaching. Appl. Environ. Microb. 64, 2743–2747.
Germann, K., 1973. Deposition of manganese and iron carbonates and silicates in Liassic Marls of the Northern Limestone Alps (Kalkalpen). Int. Union Geol. Sci. 3, 129–138.
Greenslate, J., 1974. Microorganisms participate in the construction of manganese nodules. Nature 249, 181–183.
Gu, G.H., Sun, X.J., Hu, K.T., Li, J.H., Qiu, G.Z., 2012. Electrochemical oxidation behavior of pyrite bioleaching by *Acidthiobacillus ferrooxidans*. Trans. Nonferr. Metal Soc. 22, 1250–1254.
Gu, G.H., Hu, K.T., Zhang, X., Xiong, X.X., Yang, H.S., 2013. The stepwise dissolution of chalcopyrite bioleached by *Leptospirillum ferriphilum*. Electrochim. Acta 103, 50–57.
Hackl, R.P., Dreisinger, D.B., Peters, E., King, J.A., 1995. Passivation of chalcopyrite during oxidative leaching in sulfate media. Hydrometallurgy 39 (1–3), 25–48.
Harneit, K., Goksel, A., Kock, D., Klock, J.H., Gehrke, T., Sand, W., 2006. Adhesion to metal sulfide surfaces by cells of *Acidithiobacillus ferrooxidans*, *Acidithiobacillus thiooxidans* and *Leptospirillum ferrooxidans*. Hydrometallurgy 83, 245–254.
Heinrich, H.T.M., Bremer, P.J., Daughney, C.J., McQuillan, A.J., 2007. Acid–base titrations of functional groups on the surface of the thermophilic bacterium Anoxybacillus flavithermus: comparing a chemical equilibrium model with ATR-IR spectroscopic data. Langmuir 23, 2731–2740.
Jensen, D.L., Boddum, J.K., Tjell, J.C., Christensen, T.H., 2002. The solubility of rhodochrosite ($MnCO_3$) and siderite ($FeCO_3$) in anaerobic aquatic environments. Appl. Geochem. 17, 503–511.
Kim, D.G., Jiang, S., Jeong, K., Ko, S.O., 2012. Removal of 17 alpha-Ethinylestradiol by biogenic manganese oxides produced by the *Pseudomonas putida* strain MnB1. Water Air Soil Poll. 223, 837–846.
Kosterov, A., Frederichs, T., von Dobeneck, T., 2006. Low-temperature magnetic properties of rhodochrosite ($MnCO_3$). Phys. Earth Planet In. 154, 234–242.
Lin, H.K., Say, W.C., 1999. Study of pyrite oxidation by cyclic voltammetric, impedance spectroscopic and potential step techniques. J. Appl. Electrochem. 29, 987–994.
Liu, Y., Dang, Z., Lu, G.N., Wu, P.X., Feng, C.H., Yi, X.Y., 2011. Utilization of electrochemical impedance spectroscopy for monitoring pyrite oxidation in the presence and absence of *Acidithiobacillus ferrooxidans*. Miner. Eng. 24, 833–838.
Lopez-Juarez, A., Gutierrez-Arenas, N., Rivera-Santillan, R.E., 2006. Electrochemical behavior of massive chalcopyrite bioleached electrodes in presence of silver at 35 °C. Hydrometallurgy 83, 63–68.
Luo, Y.X., Millero, F.J., 2003. Solubility of rhodochrosite ($MnCO_3$) in NaCl solutions. J. Solution Chem. 32, 405–416.
Miller, A.Z., Dionisio, A., Braga, M.A.S., Hernandez-Marine, M., Afonso, M.J., Muralha, V.S.F., Herrera, L.K., Raabe, J., Fernandez-Cortes, A., Cuezva, S., Hermosin, B., Sanchez-Moral, S., Chamine, H., Saiz-Jimenez, C., 2012. Biogenic Mn oxide minerals coating in a subsurface granite environment. Chem. Geol. 322, 181–191.
Okazaki, M., Sugita, T., Shimizu, M., Ohode, Y., Iwamoto, K., deVrinddeJong, E.W., deVrind, J.P.M., Corstjens, P.L.A.M., 1997. Partial purification and characterization of manganese-oxidizing factors of *Pseudomonas fluorescens* GB-1. Appl. Environ. Microb. 63, 4793–4799.
Okita, P.M., 1992. Manganese Carbonate Mineralization in the Molango District, Mexico. Econ Geol. Bull. Soc. 87, 1345–1366.
Pan, X.L., Wang, J.L., Zhang, D.Y., 2005. Biosorption of Pb(II) by *Pleurotus ostreatus* immobilized in alginate gel. Process Biochem. 40, 2799–2803.
Pan, X.L., Liu, J., Zhang, D.Y., 2010a. Binding of phenanthrene to extracellular polymeric substances (EPS) from aerobic activated sludge: a fluorescence study. Colloid Surf. B 80, 103–106.
Pan, X.L., Liu, J., Zhang, D.Y., Chen, X., Li, L.H., Song, W.J., Yang, J.Y., 2010b. A comparison of five extraction methods for extracellular polymeric substances (EPS) from biofilm by using three-dimensional excitation–emission matrix (3DEEM) fluorescence spectroscopy. Water SA 36, 111–116.
Pan, X.L., Liu, J., Zhang, D.Y., Song, W.J., Wu, F.C., 2010c. Binding of dicamba to soluble and bound extracellular polymeric substances (EPS) from aerobic activated sludge: a fluorescence quenching study. J. Colloid Interf. Sci. 345, 442–447.
Post, J.E., 1999. Manganese oxide minerals: crystal structures and ecomomic and environmental significance. Proc. Natl. Acad. Sci. USA 96, 3447–3454.
Rohwerder, T., Gehrke, T., Kinzler, K., Sand, W., 2003. Bioleaching review Part A: Progress in bioleaching: fundamentals and mechanisms of bacterial metal sulfide oxidation. Appl. Microbiol. Biot. 63, 239–248.
Roy, S., 1997. Genetic diversity of manganese deposition in the terrestrial geological record. Geological Society, London, Special Publications 119, 5–27.
Salerno, M.B., Li, X., Logan, B.E., 2007. Adhesion characteristics of two *Burkholderia cepacia* strains examined using colloid probe microscopy and gradient force analysis. Colloid Surf. B 59, 46–51.
Savenko, A.V., 2005. Solubility of rhodochrosite and speciation of manganese(II) in seawater. Geochem. Int. 43, 816–820.
Schiller, C.A., Strunz, W., 2001. The evaluation of experimental dielectric data of barrier coatings by means of different models. Electrochim. Acta 46, 3619–3625.
Shi, S.Y., Fang, Z.H., Ni, J.R., 2005. Electrochemical impedance spectroscopy of marmatite-carbon paste electrode in the presence and absence of *Acidithiobacillus ferrooxidans*. Electrochem. Commun. 7, 1177–1182.
Tang, Y.Z., Zeiner, C.A., Santelli, C.M., Hansel, C.M., 2013. Fungal oxidative dissolution of the Mn(II)-bearing mineral rhodochrosite and the role of metabolites in manganese oxide formation. Environ. Microbiol. 15, 1063–1077.
Tebo, B.M., Bargar, J.R., Clement, B.G., Dick, G.J., Murray, K.J., Parker, D., Verity, R., Webb, S.M., 2004. Biogenic manganese oxides: properties and mechanisms of formation. Annu. Rev. Earth Planet. Sci. 32, 287–328.

Tebo, B.M., Johnson, H.A., McCarthy, J.K., Templeton, A.S., 2005. Geomicrobiology of manganese(II) oxidation. Trends Microbiol. 13, 421–428.
Tourney, J., Ngwenya, B.T., Mosselmans, J.W.F., Tetley, L., Cowie, G.L., 2008. The effect of extracellular polymers (EPS) on the proton adsorption characteristics of the thermophile *Bacillus licheniformis* S-86. Chem. Geol. 247, 1–15.
Tributsch, H., 2001. Direct versus indirect bioleaching. Hydrometallurgy 59, 177–185.
Wang, H.W., Chen, F.L., Mu, S.Y., Zhang, D.Y., Pan, X.L., Lee, D.J., Chang, J.S., 2013. Removal of antimony (Sb(V)) from Sb mine drainage: biological sulfate reduction and sulfide oxidation-precipitation. Bioresour. Technol. 146, 799–802.
Watling, H.R., 2006. The bioleaching of sulphide minerals with emphasis on copper sulphides – a review. Hydrometallurgy 84 (1–2), 81–108.
Zeng, W.M., Qiu, G.Z., Zhou, H.B., Liu, X.D., Chen, M., Chao, W.L., Zhang, C.G., Peng, J.H., 2010. Characterization of extracellular polymeric substances extracted during the bioleaching of chalcopyrite concentrate. Hydrometallurgy 100, 177–180.
Zeng, W.M., Qiu, G.Z., Zhou, H.B., Chen, M.A., 2011. Electrochemical behaviour of massive chalcopyrite electrodes bioleached by moderately thermophilic microorganisms at 48 °C. Hydrometallurgy 105, 259–263.
Zhang, D.Y., Wang, J.L., Pan, X.L., 2006. Cadmium sorption by EPSs produced by anaerobic sludge under sulfate-reducing conditions. J. Hazard. Mater. 138 (3), 589–593.
Zhang, D.Y., Pan, X.L., Mostofa, K.M.G., Chen, X., Song, W.J., Wu, F.C., Mu, G.J., Song, W.J., Liu, J., 2010. Complexation between Hg(II) and biofilm extracellular polymeric substances: an application of fluorescence spectroscopy. J. Hazard. Mater. 175, 359–365.
Zhang, D.Y., Lee, D.J., Pan, X.L., 2013. Desorption of Hg(II) and Sb(V) on extracellular polymeric substances: effects of pH, EDTA, Ca(II) and temperature shocks. Bioresour. Technol. 128 (2013), 711–715.